METEOROLOGICAL APPLICATIONS
Meteorol. Appl. **20**: 287–295 (2013)
Published online 31 January 2012 in Wiley Online Library
(wileyonlinelibrary.com) DOI: 10.1002/met.1282

An automated nowcasting system of mesoscale convective systems for the Mediterranean basin using Meteosat imagery. Part I: System description

Stavros Kolios[a]* and Haralambos Feidas[b]
[a] *Department of Geography, University of the Aegean, Mytilene 81100, Greece*
[b] *Department of Meteorology and Climatology, Aristotle University of Thessaloniki, Greece*

ABSTRACT: This study presents the methodologies used to develop a nowcasting system of Mesoscale Convective Systems (MCSs) over the Mediterranean region on the basis of Meteosat Second Generation (MSG) imagery. The nowcasting system is an algorithm that detects and tracks MCSs in Meteosat images and then forecasts the movement and the evolution of the physical properties of a selected MCS through its entire lifecycle, at 15 min intervals. The forecasting procedure combines a linear extrapolation method of the MCS life cycle history and information extracted from conceptual models. As a final output, the system generates a complete life cycle forecast of the temporal evolution of several physical characteristics of the MCS, such as areal extent, displacement, mean brightness temperature and convective potential, and visualizes the forecast by drawing ellipses that represent the MCS with 15 min time steps. Forecasts of a complete life cycle are updated every 15 min in accordance to the acquisition of a new satellite image.

KEY WORDS forecasting algorithm; mesoscale convective system; Meteosat Second Generation; thermal infrared satellite imagery; Mediterranean basin

Received 26 April 2011; Revised 29 July 2011; Accepted 21 October 2011

1. Introduction

Mesoscale Convective Systems (MCSs) are of great importance due to their direct impact on human life and property. They produce severe weather conditions such as heavy rain, hail, strong winds, tornadoes, lightning, and flooding that can significantly impact human activities (Fujita, 1986; Maddox *et al*., 1986; Rutledge *et al*., 1993; Romero *et al*., 2000; Gaye *et al*., 2005; Correoso *et al*., 2006). MCSs mainly occur over tropical and midlatitude regions taking many different sizes and shapes (Jirak *et al*., 2003; Houze, 2004). Their horizontal dimensions extend a few hundred kilometres in one direction, reaching many thousand kilometres in some cases (Orlanski, 1975; Fujita, 1981; Roca and Ramanathan, 1999) and their lifecycles range approximately from a few hours to as long as 1–2 days (Hodges and Thorncroft, 1997; Morel and Senesi, 2002a, 2002b). The forecast of these systems is difficult and complicated not only due to their small scale internal dynamics but also because they can develop under various favourable conditions depending on topography, synoptic weather conditions, the humidity of the atmosphere, the atmospheric instability, the wind shear and on many other factors.

Mesoscale convective models have been widely used to simulate the convective processes involved in the development of MCSs (Rutledge, 1991). However, these models are not effective in developing and organizing convection at the correct time and location due to the small-scale nature of many of the features that contribute to the convection initiation and development (Kain and Fritsch, 1992; Stensrud and Fritsch, 1994a, 1994b; Toth *et al*., 1998; Buizza *et al*., 1999). Moreover, although mesoscale numerical models offer a satisfactory spatial resolution nowadays, this resolution still remains coarser than that of the geostationary satellites.

Ground-based weather radars are commonly used to provide accurate information about the presence, the shape and the structure of MCSs (Doswell *et al*., 1996; Jirak *et al*., 2003; Rigo and Llasat, 2004). Radar data were the basis for various nowcasting methods focusing on convective patterns (e.g. Rigo *et al*., 2010; Chaudhuri and Middey, 2011). They provide, however, incomplete spatial coverage over remote land and oceanic areas.

The use of modern geostationary meteorological satellites with their fine time (15 min) and space (3 km at the sub-satellite point) sampling and large geographical coverage has become an excellent alternative way to face the uncertainness and the restrictions of many numerical models and radars in MCS forecasting. For example, the spatio-temporal resolution of the Meteosat Second Generation (MSG) data provides the capability to track and forecast the rapid evolution of dynamic phenomena such as MCSs. The tracking quality of rapidly developing convective cells can be further improved with the 5 min temporal resolution offered by Meteosat Rapid Scanning Service (RSS) as demonstrated by Aoshima *et al*. (2008).

In general a short-range (0–12 h) MCS forecasting procedure based on satellite or radar data can be implemented in three main stages (Riosalido, 1996): early warning of convection, detection of convective cells and forecasting their movement and evolution. For the third stage (forecasting of movement and evolution) most techniques often rely on linear extrapolation or advection of satellite and radar data to produce very short-range forecasts (Collier, 1989; Brown *et al*., 1994). The linear extrapolation of recent trends, however, cannot deal with the different development stages, splitting and merging of the convective systems.

Therefore, new approaches were adopted to give information about the behaviour and the development stage of convective

* Correspondence to: S. Kolios, Department of Geography, University of the Aegean, University Hill, Mytilene 81100, Greece.
E-mail: stavroskolios@yahoo.gr

events during very short-range forecasting, like the incorporation of conceptual life cycle models. In this context, many studies combined linear extrapolation techniques with object-oriented conceptual life cycle models of convective clusters to provide very short-range forecasts of the movement and evolution of an existing convective system (Zipser, 1982; Hand and Conway, 1995; Riosalido *et al*., 1998). In a recent study, Puca *et al*. (2005) developed a fully automated system called 'NEFODINA' that uses a linear extrapolation method along with a neural network algorithm to forecast the MCS evolution for the next 30 min over the Italian peninsula and its surroundings based on multispectral MSG imagery. More recently, Vila *et al*. (2008) combined linear extrapolation methods with a MCS life cycle model to develop the 'ForTraCC' algorithm for tracking and forecasting radiative and morphological properties of MCSs up to 120 min over South America.

Studies for developing very short-range forecasts of MCS properties over the Mediterranean basin remain rare. Readers may refer to the studies of Riosalido *et al*. (1998), Puca *et al*. (2005) and Morel and Senesi (2002a) who developed automated systems using Meteosat data with application areas the Spain, Italy and central Europe, respectively. A widely used nowcasting system is the Rapidly Developing Product (RTD) developed under the Satellite Application Facility in support to Nowcasting and Very Short Range Forecasting (SAFNWC) (http://www.nwcsaf.org) This system, however, is limited to the identification, tracking and monitoring of intense convective systems using MSG data without forecasting their movement and evolution.

Mediterranean basin, however, is of high interest due to the severe convective activity occurring particularly during the warm season of the year (from April to October) (Funatsu *et al*., 2009). These convective systems often develop over remote land and sea areas, where the lack of conventional observation networks makes the use of satellite imagery essential for monitoring and forecasting mesoscale convection in the Mediterranean basin.

The purpose of this study is to develop an automated algorithm for tracking and very short-range forecasting of the physical properties of MCSs through their entire life cycle over the entire Mediterranean basin and its surroundings using the infrared multispectral information of the MSG satellite. The basic objectives are twofold: identification, monitoring and tracking of MCSs as well as forecasting their movement and evolution for their entire life cycle.

Part II of this article (Kolios and Feidas, 2012) presents an assessment of the performance of this algorithm.

2. Application area and data

The forecasting system produces analyses and forecasts over a fixed domain on the MSG projection system, covering the Mediterranean basin and its surroundings (from 28°N to 50°N, and 5°W to 35°E) (Figure 1). The system uses data obtained with the Spinning Enhanced Visible & InfraRed Imager (SEVIRI) instrument on board MSG satellites with a 15 min temporal sampling rate and about 3 km × 3 km spatial resolution at the sub-satellite point, reaching 5 × 6 km^2 at the easternmost limit of the area of study. The dataset used includes images from two spectral channels of SEVIRI, with centres at the thermal infrared (10.8 μm) and water vapour (6.2 μm) spectral region.

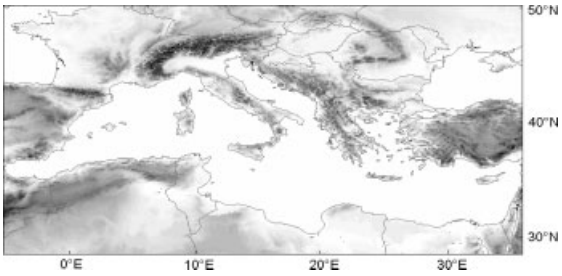

Figure 1. The system domain and orography.

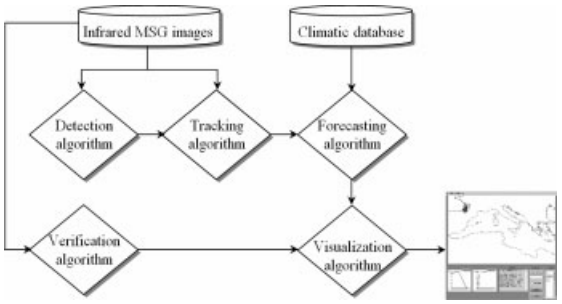

Figure 2. A simplified flow chart of the methodology of the system.

3. The forecasting system

The forecasting system consists of five main procedures, shown schematically in Figure 2: (1) an MCS detection algorithm based on size and brightness temperature thresholding of MSG infrared data which also computes a set of MCS radiative and structural properties, (2) an algorithm for tracking the identified MCSs based on their area overlap on consecutive images, (3) a forecast procedure relying on a linear extrapolation technique combined with a MCS conceptual life cycle model derived from the local climatology, (4) a verification module that provides real-time statistical verification measures for each forecast cycle of a particular MCS, and (5) a visualization routine to visualize the forecasts. The developed algorithms have been implemented in the VB.NET programming language.

3.1. The detection algorithm

The first procedure aims at identifying cloud tops in the infrared imagery based on a size and temperature threshold. This approach relies on the premise that convective cloud tops are strongly associated to low brightness temperatures in infrared satellite data. The algorithm detects mesoscale cloud cells, defined as clusters of contiguous pixels with brightness temperatures lower than 228 K and areal extent over 100 km^2 in the 10.8 μm channel. The 228 K is a temperature threshold proposed by Kolios and Feidas (2007, 2010) who used a set of lightning data to identify MCSs over the Mediterranean region. This temperature threshold was also used by Morel and Senesi (2002a, 2002b) for establishing the climatology of MCS over Europe and is very close to the 221 K threshold used by Garcia-Herrera *et al*. (2005) over the Iberian Peninsula. It is quite a low temperature that enables us to locate the areas of active deep convection that often reach or overrun the highest levels of the tropopause (Johnson *et al*., 1990; Roca and Ramanathan, 1999; Setvak *et al*., 2008).

The area threshold of 100 km^2 set for the first detection of an MCS was also found by Kolios and Feidas (2007, 2010) to best identify the small convective systems prevailing over

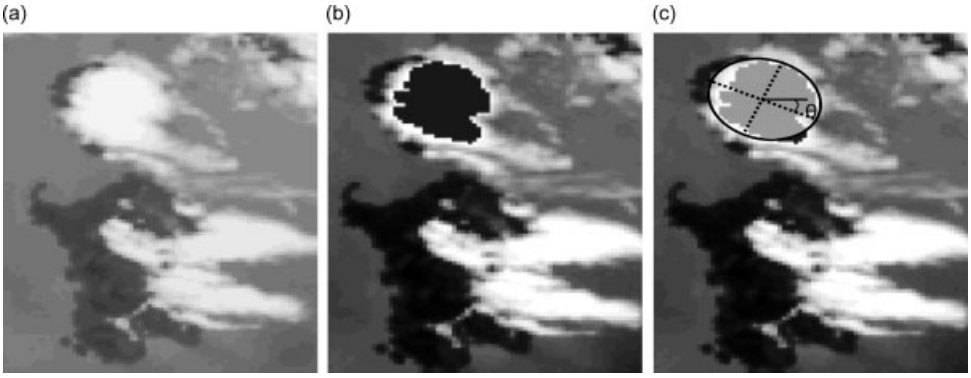

Figure 3. An example of MCS detection over Corsica (France) and Sardinia (Italy). (a) The MSG infrared image at the 10.8 μm on 13 July 2005, at 1330 UTC. (b) The same image with the detected MCS coloured in black. (c) The best fitting ellipse that approximates the shape of the MCS. Dotted lines indicate the major and minor axes of the ellipse and θ the orientation of the ellipse.

Table 1. Main MCS parameters calculated by the detection algorithm and estimated by the forecasting algorithm.

Parameter	Type	Definition
Areal extent	Morphological	The area (km^2) covered by the MCS, which represents the MCS size.
Semi-axis length	Morphological	The length (km) of the major semi-axis of the best fitted ellipse.
Location of centre of mass	Positional	Co-ordinates of the centre of the ellipse that represents the forecasted MCS.
Mean brightness temperature	Radiative	MCS mean brightness temperatures at the infrared (10.8 μm) and water vapour (6.2 μm) channels
Brightness temperature of 10% coldest MCS pixels	Radiative	The brightness temperature at the infrared (10.8) channel corresponding to the 10% coldest MCS pixels
Convective potential	Radiative	The percentage of MCS pixels with positive brightness temperature difference between water vapour (6.2 μm) and infrared (10.8 μm) channels (Kolios and Feidas, 2010)

the Mediterranean basin. Consistent and continuous tracking of these small MCSs during the early phases of development is ensured by the high temporal sampling of SEVIRI data (15 min). Most of the detected cloud cells using the 100 km^2 area threshold reach their maximum extend in the *meso-β* scale (with typical dimensions ranging from 25 to 250 km). An example of MCS detection over the central Mediterranean is presented in Figure 3.

In order to represent a detected cloud cell as a simplified object, its shape is approximated by a best-fit ellipse, as proposed by Zittel (1976) and Dixon and Wiener (1993) (Figure 3(c)). In this way, the shape of the cloud cells is described by the length of the major and minor axis of the ellipse and the orientation of the major axis relative to the x-axis.

Finally, some basic structural and radiative parameters are computed for each detected cloud cell. The parameters of importance for the forecasting system are described in Table 1. An extensive description of all the parameters computed by the system is provided in Feidas (2003) and Kolios and Feidas (2010).

3.2. The tracking algorithm

The tracking algorithm allows building trajectories of cloud cells identified by the detection algorithm. The tracking methodology is based on the area overlap method presented by Feidas (2003). This technique matches cloud cells in successive images by comparing the detected cells in the current image with those of the previous image and determining their overlap. Then, a 'trajectory' is defined for each MCS by linking its matching cells in consecutive images. In our case, only trajectories with a lifetime longer than 2 h are considered. The tracking procedure also takes into account any likely mergers and splits of a cell following the criteria set by Feidas (2003).

At this point, the motional properties of the MCS are calculated (displacement vector and velocity) according to the cloud cell displacement in the last two sequential images. Finally, for each trajectory (MCS) extracted by the tracking algorithm, a time series of the morphological, positional and radiative properties of the cloud cells forming the trajectory is calculated and stored for further use.

3.3. The forecasting algorithm

The forecasting procedure generates forecasts of the movement and evolution of the physical properties of a MCS through its entire lifecycle at 15 min intervals, by combining a linear extrapolation of recent trends with a MCS conceptual life cycle model derived from the local climatology (Kolios and Feidas, 2010). This climatology was build by Kolios and Feidas (2010) to study the climatic characteristics of warm season isolated MCSs over the Mediterranean basin using MSG infrared imagery.

Based on the results of this climatology, conceptual life cycle models for each MCS parameter and statistical relationships among these parameters were derived and then used to forecast the movement and evolution of an existing MCS. The dataset used to build the MCS climatology consists of 4718 isolated MCSs, namely single convective cells not affected by splitting

or merging with neighbour systems during their life cycle. This is to ensure that the estimated conceptual life cycle model is characteristic of a typical MCS with a complete life cycle in the area of interest. This sample of isolated MCSs represents the 22.4% of the 20 992 MCSs identified by the tracking algorithm over the Mediterranean basin during the warm season of a 3 year period. Each MCS in the sample satisfies the following criteria: (1) the MCSs' generation and dissipation must be spontaneous (without splitting or merging), (2) the MCSs have at least a 2-h lifetime, and (3) the MCSs lie entirely inside the study area (Figure 1) during their lifetime (Kolios and Feidas, 2010).

The mean lifetime of the 4718 MCS used to construct the conceptual life-cycle models was 180 min (median: 165 min) with a small standard deviation of less than 30 min (Kolios and Feidas, 2010). These results are in close agreement with the statistics of the isolated thunderstorms (mean lifetime of 204 min and median of 192 min) examined by Rigo *et al.* (2010) for the warm season in the NW Mediterranean using radar and lightning data. Regarding to the duration of the development and dissipitation phases Rigo *et al.* (2010) were concluded that they last the same (mean duration of 48 min at both of them), which is consistent with the conceptual life-cycle model of the areal extent where the phase of a typical MCS changes in the middle of its lifetime (Kolios and Feidas, 2012).

The developed forecasting methodology is implemented in four steps. The first three steps are related to the forecast of (1) the life cycle phase and duration, (2) the MCS displacement and shape, and (3) the evolution of the physical properties of a given MCS, whereas the last step, (4), deals with the real time verification of the forecasts.

3.3.1. *MCS life cycle duration*

The estimation of the MCS life cycle duration is a fundamental issue in forecasting its evolution. For this reason, it is important to find a connection between the life cycle duration and a parameter that can be easily calculated during the first time of detection (initiation) or at least at the early stages of the MCS development.

By investigating the statistical relationships between MCSs lifecycle duration t_d and the mean evolution of basic physical parameters during their lifetime derived by the database built by Kolios and Feidas (2010), a general relationship between t_d and the maximum areal extent A_{max} (Figure 4(a)) was found, which can be approximated by the exponential equation:

$$t_d = a_1(A_{max} - b_1)^{c_1} \quad (1)$$

where $a_1 = 1.98$, $b_1 = 2198.37$ and $c_1 = 0.21$ are constants derived by fitting the equation to the data of the MCS database (see Figure 4(a)). In general, convective systems with a small maximum areal extent have short life duration and the MCS lifetime increases as its maximum areal extent increases. For A_{max} larger than 6000 km^2 the relationship tends to be asymptotic. The very high correlation co-efficient ($R = 0.95$) suggests that, within error limits, the maximum areal extent could serve as an indicant of the MCS life cycle duration, and that the average relationship can be simulated by the exponential function of Equation (1). This relation has also been pointed out in other studies dealing with MCS characteristics (Morel and Senesi, 2002b; Garcia-Herrera *et al.*, 2005).

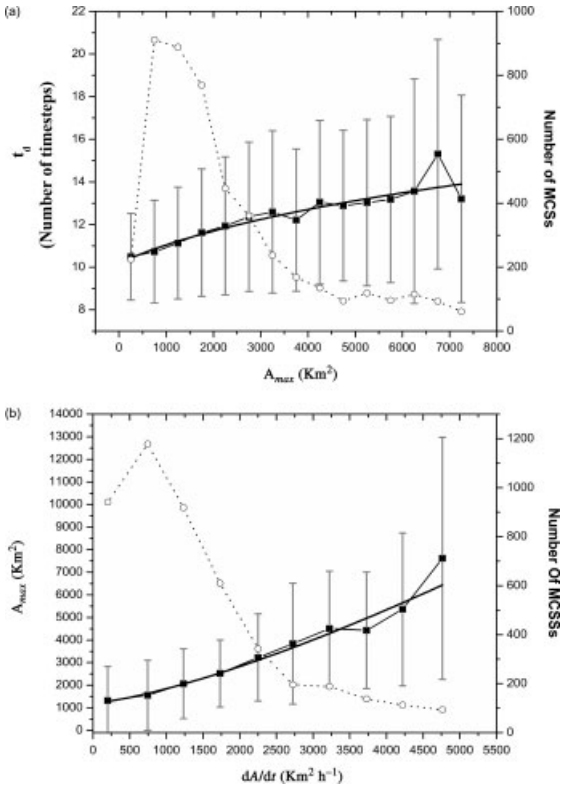

Figure 4. (a) Duration t_d (in number of 15 min time steps) of the MCS lifecycle as a function of the maximum areal extent A_{max}. (b) Maximum areal extent A_{max} as a function of the areal expansion rate dA/dt. Values at the *x-axis* are grouped in class intervals. The fitted curve, the associated standard deviations and number of cases are also plotted. –▪–: Parameter; —: standard deviation; ▬: fitted curve; ···: Number of MCSs.

The statistical relationships between the physical properties of the MCSs also revealed a significant statistical correlation ($R = 0.98$) between the areal expansion rate dA/dt at the initial time (between the first two time steps) of the MCS lifecycle and its maximum areal extent A_{max} (Figure 4(b)). On average, the maximum areal extent increases exponentially with the areal expansion rate according to the following equation:

$$A_{max} = a_2 + b_2\left(\frac{dA}{dt}\right)^{c_2} \quad (2)$$

where $a_2 = 1369.93$, $b_2 = 0.0011$ and $c_2 = 1.814$ are also constants derived by fitting the relation to the data of the MCS database (see Figure 4(b)). In general, the growth of convective systems with a weak areal expansion rate during the initiation phase leads to a small maximum areal extent of the MCS.

This connection is reasonable from a satellite point of view, since the growth rate of these convective systems can be represented by their areal expansion rate in consecutive images. In this context, the growth rate during the first stages of the MCS development can be associated not only to the areal expansion rate of this system but also to its maximum areal extent, given that the later is the outcome of the MCS convective activity during its growing phase.

In this concept, the forecasting system can provide timely forecasts of life cycle duration after the first detection of a MCS by a two-step procedure. First, the areal expansion rate dA/dt at the initiation time of the MCS lifecycle is calculated in order to estimate the maximum areal extent A_{max} with Equation (2).

The estimated $A_{\max}$ value is then used to estimate the life cycle duration t_d of the MCS (in a number of 15 min time steps) with Equation (1).

3.3.2. MCS displacement

The forecast of the MCS displacement refers to the estimation of the co-ordinates of the centre of the ellipse that represents the forecasted MCS. The methodology used is a modified version of the technique devised by Vila *et al*. (2008) who based their estimations on the displacement of the geometrical centre of mass (the temperature-weighted centre using the brightness temperature of each cloud pixel as a weight) in the last two time steps. In this case, the co-ordinates of the centre of the ellipse representing the forecasted MCS are derived using a displacement vector that is an average of the MCS displacement in the last time step and the mean displacement during the lifetime of the MCS. This procedure is presented graphically in Figure 5.

The displacement $\mathbf{V}_t$ in the last time step is a vector joining the geometrical centres of mass of the MCS at times $t - \Delta t$ and t. In order to make the forecast as consistent as possible to the mean past motion of the system and smooth possible abrupt or non-realistic MCS displacements introduced by splits and mergings, the mean displacement vector $\mathbf{V}_m$ was used to adjust the linearly extrapolated displacement vector $\mathbf{V}_t$. To this end, a displacement vector $\mathbf{V}$ during the entire life cycle of the MCS is calculated considering the positions of the centre of mass of the MCS at the present time t and the time of first detection $t - n\Delta t$, where n is the number of the time steps corresponding to the life history of the system ($n = 2$ in the case of Figure 5). The mean displacement vector $\mathbf{V}_m$ is computed as the one nth of the displacement vector $\mathbf{V}$ during the entire life cycle:

$$V_{\mathrm{m}} = \frac{1}{n} \times V \tag{3}$$

The forecasted MCS displacement vector $\mathbf{V}_{t+\Delta t}$ for the next time step $t + \Delta t$ is estimated by the equation:

$$V_{t+\Delta t} = \frac{1}{2} \times (V_t + V_{\mathrm{m}}) \tag{4}$$

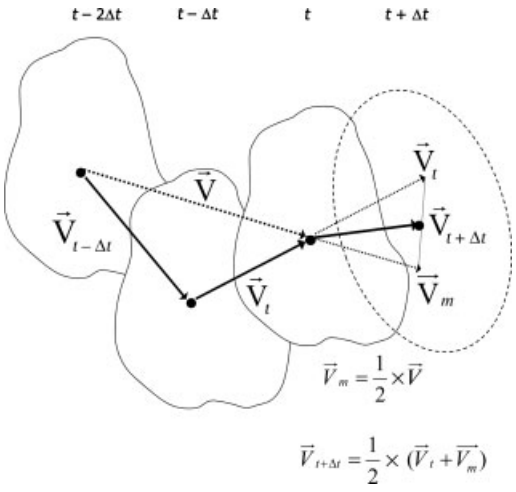

Figure 5. Graphical representation of the method used to forecast the displacement of the MCS, using the positions of the centre of mass of the MCS in three consecutive steps ($t - 2\Delta t$, $t - \Delta t$ and t). The forecasted position of the MCS is indicated with the dashed ellipse.

The estimated displacement $\mathbf{V}_{t+\Delta t}$ is used to forecast the displacement $\mathbf{V}_{t+2\Delta t}$ for the next time step $t + 2\Delta t$ by applying the same methodology. This procedure is implemented to all the next time steps until the end of the estimated MCS lifecycle duration.

3.3.3. Evolution of MCS physical parameters

This section aims at developing a general model to simulate and then forecast the evolution of the MCS physical parameters. Forecasts can be made for several physical parameters. The MCS parameters of importance to the forecasting technique are (Table 1): two parameters of the best fitted ellipse (location of the centre and axis length), the areal extent, the mean brightness temperatures, the 10% coldest temperature and the convective potential.

The convective potential is a measure of the convective intensity of the MCS expressed as the percentage of MCS pixels with positive brightness temperature difference between water vapour (6.2 μm) and infrared (10.8 μm) channels (Kolios and Feidas, 2010). Positive differences may be obtained when deep convective clouds penetrate into the stratosphere (Fritz and Laszlo, 1993; Tjemkes *et al*., 1997). One possible explanation for this phenomenon is the presence of stratospheric water vapour due to overshooting clouds. Nevertheless, the 'warm' WV pixel phenomenon could also have different causes such as a previous very active cell, calibration uncertainties and variability of the viewing angle of geostationary instrumentation (Lattanzio *et al*., 2005). Besides, Bedka *et al*. (2010) have shown that the use of the 'warm' WV pixels is not always a safe criterion to characterize deep convection and especially overshooting tops. The use of this difference in combination with other brightness temperature differences (e.g. 3.8–10.8 μm, 10.8–12.1 μm) could lead to a substantial improvement of the characterization of MCSs' convective intensity, but this is a topic for future work.

The aforementioned parameters are forecasted for the entire life cycle duration estimated in the previous step, by combining a simple linear extrapolation method with a conceptual life-cycle model representing the mean evolution of the parameter. Simple linear extrapolation techniques have been proved to be very efficient in very short-range forecasting when information about the development stage and the behaviour of a MCS is provided by a conceptual life cycle model (Zipser, 1982; Hand and Conway, 1995; Riosalido *et al*., 1998).

The MCS life-cycle model used in this procedure has been obtained by previous 3 year satellite climatology of isolated warm season MCSs built for the Mediterranean area (Kolios and Feidas, 2010). Life-cycle model for each parameter is derived as a mean of nearly 4700 isolated MCSs after being normalized by the maximum value of the parameter and life cycle duration (Figure 6). The conceptual life cycle model was introduced to define the life cycle phase of a given MCS (growth or decay) and simulate the evolution of its parameters during the decay phase. Given the large variability of each parameter in the dataset, it is expected that these estimates to diverge from reality in the cases of individual MCSs that deviate from the normal. This statistical approach, however, works in improving the results of a simple linear extrapolation method and extending the forecast period.

Figure 6(a) shows the life cycle model of cloud cell area. Using this model two main stages or phases in the MCS life cycle can be defined: a phase in which area is growing (growing phase) and a stage in which area is decreasing (decaying phase). The transition from the one phase to the other occurs at the

(normalized) time when the area reaches its maximum value. Both phases have the same duration, a result that is consistent with the finding of Rigo *et al*. (2010).

The life cycle models for two radiative parameters (brightness temperature at the 10.8 μm channel and convective potential) and one morphological parameter (major semi-axis of the ellipse fitted to the MCS) are also shown in Figure 6. These models exhibit a main characteristic commonly observed in many studies, that is the time lag between the maximum (minimum) values of the radiative parameters and the peak in the cloud cell area (Arnaud *et al*., 1992; Riosalido *et al*., 1998; Feidas and Cartalis, 2001). The minimum brightness temperatures occur first, followed by the peak of the cloud area. Given that brightness temperatures reflect cloud-top height, this time lag indicates that MCSs grow vertically first and horizontally thereafter.

From the life cycle model of each parameter and the MCS life cycle duration estimated in the previous step, the time t_o of the transition between the growing and the decaying phase can be estimated, which could be different for each parameter (Figure 6).

The probable evolution of a given parameter X during the growing phase of a MCS is determined by a linear regression between the history data of the parameter X_t, $X_{t-\Delta t}$, $X_{t-2\Delta t}$, ..., $X_{t-n\Delta t}$ and time t, where t is the present, $t-\Delta t$, $t-2\Delta t$, ... are time steps in the past, and n is the elapsed time steps from the time of first detection. The linear regression fits a straight line to the history data with its slope $\mathrm{d}X/\mathrm{d}t$ being a mean rate of change for the parameter X. The forecast model uses the current value X_t and the estimated mean rate $\mathrm{d}X/\mathrm{d}t$ of change to forecast the value $X_{t+n\Delta t}$ at the nth time step in the future according to equation:

$$X_{t+n\Delta t} = X_t + \frac{\mathrm{d}X}{\mathrm{d}t} n\Delta t \tag{5}$$

where Δt is the temporal sample rate of MSG.

This linear extrapolation is implemented up to the end of the growing phase. The duration of the growing phase is estimated by multiplying the estimated lifetime (t_d) of the MCS with the normalized transition time (t_o) from the growing to the decaying phase derived by the life cycle model (Figure 6).

The forecast of parameter X during the decaying phase is based on a new linear equation with a slope $\mathrm{d}X/\mathrm{d}t$ that is proportional to the slope $\mathrm{d}X_n/\mathrm{d}t_n$ of the straight line AB connecting the two points of the curve of the normalized life cycle model corresponding to the start and the end of the decaying phase (Figure 6(a)):

$$X_{t+n\Delta t} = X_o + \frac{\mathrm{d}X}{\mathrm{d}t} n\Delta t \tag{6}$$

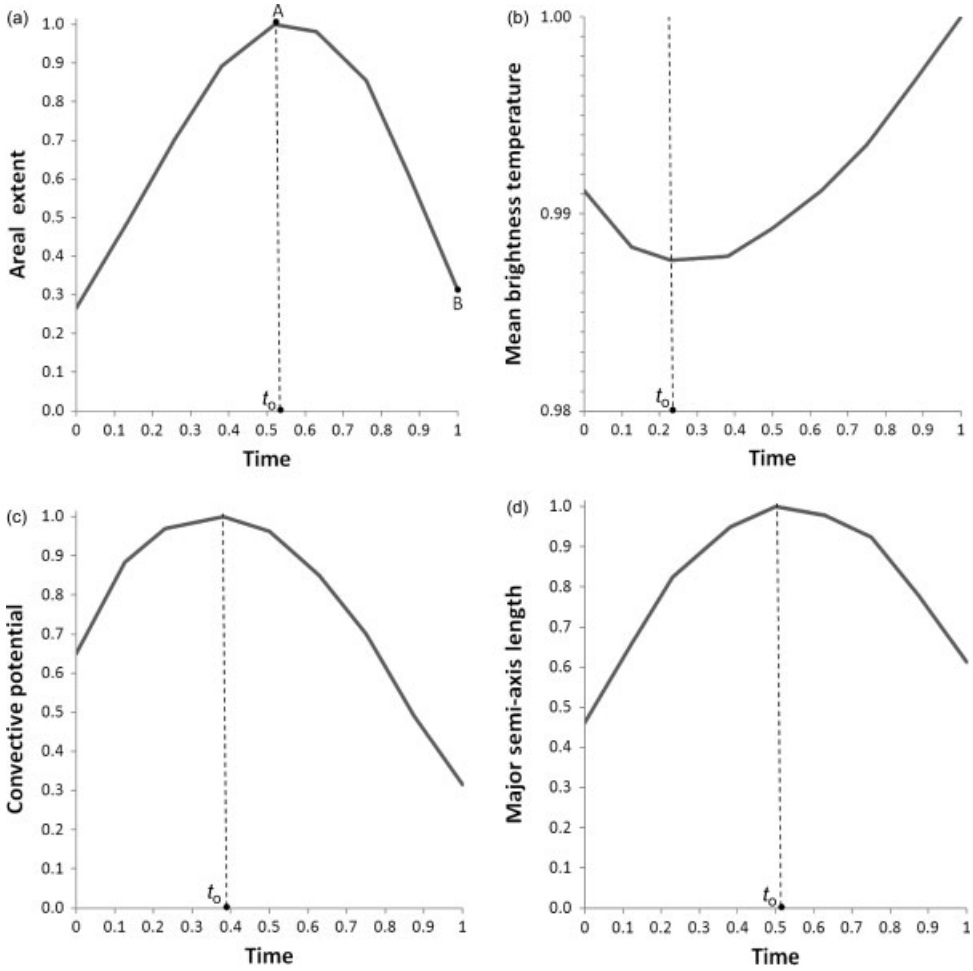

Figure 6. MCS normalized life cycle model for four parameters: (a) areal extent, (b) mean brightness temperature at the 10.8 μm, (c) convective potential, and (d) major semi-axis length of the ellipse fitted to the MCS. The dashed line indicates the transition time (t_o) from the growing to the decaying phase for each parameter.

where X_o is the value of the parameter X given by Equation (5) at the end of the growing phase, t_d is the estimated life cycle duration, n is the number of time steps in the future counting from the transition time t_o between the growing and the decaying phase, and dX/dt is the slope of the fitting line in the normalized life cycle given by:

$$\frac{dX}{dt} = \frac{dX_n}{dt_n}\frac{X_o}{t_d} \tag{7}$$

The application of this linear equation stops when time $n\Delta t$ reaches the estimated duration t_d of the MCS.

The algorithm is able to provide a complete life cycle forecast with updates every 15 min, in accordance with the acquisition of a new satellite image. The first forecast cycle starts at one time step after the first detection of the MCS. The forecast period covers the whole (estimated) life cycle duration t_d using Equations (5) and (6) for the growing and decaying phases, respectively.

When, however, the forecast cycle enters into the decaying phase of the system, the MCS evolution is simulated using a linear extrapolation method with a straight line that best fits the history data of the parameter X during the decaying phase along with the estimated value X_d at the end of the forecasted lifetime t_d, according to the life cycle model. The value X_d is obtained when the recorded maximum (minimum) value X_o at the transition time t_t between the growing and the decaying phase is inserted into the normalized life cycle model. This value is taken into account to adjust the slope of the regression line to the life cycle model and avoid equations of straight lines that could lead to the estimation of unrealistic parameter values at the end of the forecasted lifetime t_d. This could be the case during the first forecast cycles when a small number of the parameter X history data is available, thus sometimes inducing large random departures from the general model.

The previous methodology is also implemented to forecast the shape parameters of the best fitted ellipse. As mentioned before, the co-ordinates of the centre are forecast by extrapolating the displacement of the actual centre of the MCS. The other ellipse parameters are obtained by keeping constant the orientation and estimating the major and minor axes of the ellipse. The forecast of the major semi-axis a is based on the methodology applied to forecast the other physical parameters of the MCS, which is a linear extrapolation method combined with the conceptual life cycle model of the major axis length (Figure 6(d)). The minor semi-axis b results from the forecast major semi-axis α and areal extent E using the following equation:

$$b = \frac{a}{4\pi E} \tag{8}$$

3.4. The verification algorithm

The developed system also includes an automatic verification procedure that is able to provide real-time verification statistical measures for each forecast cycle of a particular MCS. Two different methodologies were used to implement the verification procedure. The first one relies on a systematic comparison between the observed and the forecasted MCS parameters. The second methodology uses statistical parameters computed by the entries of a contingency table resulting from the comparison of the ellipses representing the observed and the forecasted MCS. A detailed description of the verification methodology is presented in Part II of this paper (Kolios and Feidas, 2012).

3.5. The visualization algorithm

The forecasting system operates in a fully automated interface which comprises a visualization routine and a series of menus through which the user is able to choose data and actions (Figure 7). After the selection of a cloud system by the user,

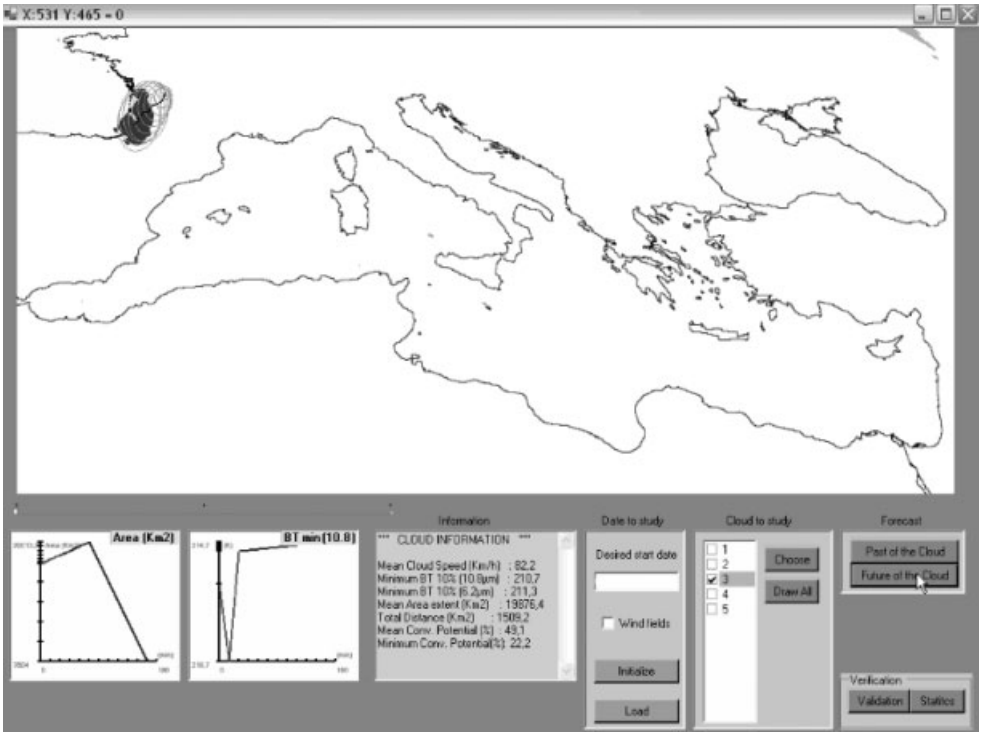

Figure 7. A snapshot of the forecasting system's interface. The forecasted life cycle of a MCS detected over the Southern France is presented by drawing ellipses and graphs.

the system visualizes the forecast by drawing the ellipse representing the MCS at the current time and the forecasted ellipses for a complete life cycle. The series of the ellipses represent the MCS evolution for a complete life cycle. At the same time, graphs with the time evolution of two selected parameters along the entire life cycle are provided by the visualization routine. Moreover, a list of the MCS properties (forecast and measured) during its life cycle is displayed as a text output in the screen and stored in 'ascii' format for further analysis.

4. Conclusions

In this study, the methodologies for detecting, tracking and very short-range forecasting of isolated MCSs over the Mediterranean region using MSG imagery are presented. The forecasting algorithm developed first to detect MCSs in satellite images and then to forecast the movement and the evolution of the physical properties of a MCS through its entire lifecycle at 15 min intervals, by combining a linear extrapolation method with information extracted from conceptual life-cycle models derived from the local climatology.

The forecasting system is fully automatic, being able to provide operational real-time forecasts updated every 15 min with the acquisition of a new satellite image. The system also includes an analytical graphical interface to visualize the forecasts and a verification routine to evaluate the forecasts' accuracy in nearly real-time mode. Verification of the forecasts is presented along with a case study in the second part of this paper (Kolios and Feidas, 2012).

The developed system should be considered as a first contribution to the nowcasting of the MCSs over the Mediterranean basin using exclusively MSG satellite data, given that the developed methodology is trained with typical cases of isolated MCS. Although the new developed scheme is applicable to every convective cloud system, the greatest benefit is obtained by MCSs with no splits – mergings during their life cycle. These typical MCSs mainly represent thermally induced convective clouds in the lower bounds of the mesoscale, which are difficult to forecast by current NWP models.

Acknowledgements

This study is a part of a research project co-financed by E.U.-European Social Fund (75%) and the Greek Ministry of Development-GSRT (25%) with the title: 'Automated system of Mesoscale Convective Systems short range forecast with the use of Meteosat imagery'. The authors would like also to express their appreciation to the anonymous reviewers for their constructive comments that helped to improve the completeness and clarity of the paper.

References

Aoshima F, Behrendt A, Bauer HS, Wulfmeyer V. 2008. Statistics of convection initiation by use of Meteosat rapid scan data during the Convective and Orographically-induced Precipitation Study (COPS). *Meteorol. Z.* **17**: 921–930.

Arnaud Y, Desbois M, Maizi MJ. 1992. Automatic tracking and characterization of African convective systems on Meteosat Pictures. *J. Appl. Meteorol.* **31**: 443–453.

Bedka K, Brunner J, Dworak R, Feltz W, Otkin J, Greenwald T. 2010. Objective satellite-based detection of overshooting tops using infrared window channel brightness temperature gradients. *J. Appl. Meteorol. Climatol.* **49**: 181–201.

Brown R, Newcomb PD, Cheung-Lee J, Ryall G. 1994. Development and evaluation of the forecast step of the FRONTIERS short-term precipitation forecasting system. *J. Hydrol.* **158**: 79–105.

Buizza R, Hollingsworth A, Lalaurette F, Ghelli A. 1999. Probabilistic predictions of precipitation using the ECMWF ensemble prediction system. *Weather Forecast.* **14**: 168–189.

Chaudhuri S, Middey A. 2011. Nowcasting thunderstorms with graph spectral distance and entropy estimation. *Meteorol. Appl.* **18**: 238–249.

Collier CG. 1989. *Applications of Weather Radar Systems*. Ellis Horwood: Chichester; 1–249.

Correoso FJ, Hernandez E, Garcia-Herrera R, Barriopedro D, Paredes D. 2006. A 3-year of cloud-to-ground lightning flash characteristics of Mesoscale convective systems over the Western Mediterranean Sea. *Atmos. Res.* **79**: 89–107.

Dixon M, Wiener DG. 1993. TITAN: thunderstorm identification, tracking, analysis and nowcasting. A Radar based methodology. *J. Atmos. Oceanic Technol.* **10**: 785–797.

Doswell CA, Brooks HE, Maddox RA. 1996. Flash flood forecasting: an ingredients-based methodology. *Weather Forecast.* **11**: 560–581.

Feidas H. 2003. A software tool for monitoring features of convective cloud systems with the use of Meteosat images. *Environ. Model. Softw.* **18**: 1–12.

Feidas H, Cartalis C. 2001. Monitoring mesoscale convective cloud systems associated with heavy storms with the use of Meteosat imagery. *J. Appl. Meteorol.* **40**: 491–512.

Fritz S, Laszlo I. 1993. Detection of water vapor in the stratosphere over very high clouds in the tropics. *J. Geophys. Res.* **98**(D12): 22959–22967.

Fujita T. 1981. Tornadoes and downbursts in the context of generalized planetary scales. *J. Atmos. Sci.* **38**: 1511–1534.

Fujita T. 1986. Mesoscale classifications: their history and their application to forecasting. In *Mesoscale Meteorology and Forecasting*, Ray PS (ed.). American Meteorological Society: Boston, MA, 18–35.

Funatsu B, Claud C, Chaboureau JP. 2009. Comparison between the large-scale environments of moderate and intense precipitating systems in the Mediterranean region. *Mon. Weather Rev.* **137**: 3933–3959.

Garcia-Herrera R, Hernandez E, Paredes D, Barriopedro D, Correoso JF, Prieto L. 2005. A MASCOTE-based characterization of MCSs over Spain, 2000–2002. *Atmos. Res.* **73**: 261–282.

Gaye A, Viltard A, De Felice P. 2005. Squall lines and rainfall over Western Africa during 1986 and 1987. *Meteorol. Atmos. Phys.* **90**: 215–224.

Hand HW, Conway BJ. 1995. An object-oriented approach to nowcasting showers. *Weather Forecast.* **10**: 327–341.

Hodges KI, Thorncroft CN. 1997. Distribution and statistics of African mesoscale convective weather systems based on the ISCCP Meteosat imagery. *Mon. Weather Rev.* **125**: 2821–2837.

Houze RA. 2004. Mesoscale convective systems. *Rev. Geophys.* **42**: 38–43.

Jirak I, Cotton W, McAnelly R. 2003. Satellite and radar survey of mesoscale convective system development. *Mon. Weather Rev.* **131**: 2428–2449.

Johnson RH, Gallus WA Jr, Vescio MD. 1990. Near tropopause vertical motion within the trailing stratiform region of a mid-latitude squall line. *J. Atmos. Sci.* **47**: 2200–2210.

Kain JS, Fritsch JM. 1992. The role of the convective "trigger function" in numerical forecasts of mesoscale convective systems. *Meteorol. Atmos. Phys.* **49**: 93–106.

Kolios S, Feidas H. 2007. Correlation of lightning activity with spectral features of clouds in Meteosat-8 imagery over the Mediterranean basin. *Proceedings of the 8th Pan-Hellenic Geographic Conference*, 4–7 October, Athens.

Kolios S, Feidas H. 2010. A warm season climatology of mesoscale convective systems in the Mediterranean basin using satellite data. *Theor. Appl. Climatol.* **102**: 29–42.

Kolios S, Feidas H. 2012. An automated nowcasting system of mesoscale convective systems for the Mediterranean basin using Meteosat imagery. Part II: Verification statistics. *Meteorol. Appl.* DOI: 10.1002/met.1281.

Lattanzio A, Watts PD, Govaerts Y. 2005. Activity Report on physical interpretation of warm water vapor pixels. EUMETSAT Technical Memorandum 14.

Maddox RA, Howard KW, Bartles DL, Rodgers DM. 1986. Mesoscale convective complexes in middle the latitudes. In *Mesoscale Meteorology and Forecasting*, Ray PS (ed.). American Meteorological Society: Boston, MA, 390–413.

Morel C, Senesi S. 2002a. A climatology of mesoscale convective systems over Europe using satellite infrared imagery. I: methodology. *Q. J. R. Meteorol. Soc.* **128**: 1953–1971.

Morel C, Senesi S. 2002b. A climatology of mesoscale convective systems over Europe using satellite infrared imagery. II. Characteristics of European mesoscale convective systems. *Q. J. R. Meteorol. Soc.* **128**: 1973–1995.

Orlanski I. 1975. A rational subdivision of scales for atmospheric processes. *Bull. Am. Meteorol. Soc.* **56**: 527–530.

Puca S, Biron D, De Leonimbus L, Melfi D, Rosci P, Zauli F. 2005. A neural network algorithm for the nowcasting of severe convective systems. *CIMSA 2005 – IEEE International Conference on Computing Intelligence for Measurement System Applications*, 20–22 July, Giardini Naxos.

Rigo T, Llasat MC. 2004. A methodology for the classification of convective structures using meteorological radar: application to heavy rainfall events on the Mediterranean coast of Iberian Peninsula. *Nat. Hazards Earth Syst. Sci.* **4**: 59–68.

Rigo T, Pineda N, Bech J. 2010. Analysis of warm season thunderstorms using an object-oriented tracking method based on radar and total lightning data. *Nat. Hazards Earth Syst. Sci.* **10**: 1881–1893.

Riosalido R. 1996. Current status and principal challenges in strong convection nowcasting in COST-78 frame. *Proceedings of COST-78 International Workshop on Improvement of Nowcasting Technology*, 25–28 March, Bologna, EUR 16996 EN; 37–47.

Riosalido R, Carretero O, Elizaga F, Martin F. 1998. An experimental tool for mesoscale convective systems nowcasting. *SAF Training Workshop on Nowcasting and Very Short Range Forecasting*, Madrid, Spain, 9–11 December, 127–135.

Roca R, Ramanathan V. 1999. Scale dependence of monsoonal convective systems over the Indian Ocean. *J. Clim.* **13**: 1286–1298.

Romero R, Doswell CA, Ramis C. 2000. Mesoscale numerical study of two cases of long-lived quasi-stationary convective systems over eastern Spain. *Mon. Weather Rev.* **128**: 3731–3751.

Rutledge SA. 1991. Middle latitude and tropical mesoscale convective systems. *Rev. Geophys.* (Suppl.) **29**: 88–97 (U.S. National Report to International Union of Geodesy and Geophysics 1987–1990, American Geophysical Union).

Rutledge SA, Williams RE, Petersen AW. 1993. Lightning and electrical structure of mesoscale convective systems. *Atmos. Res.* **29**: 27–53.

Setvak M, Lindsey TD, Novak P, Rabin RM, Wang KP, Kerkmann J, Radova M, Stastka J. 2008. Cold-Ring shaped storm in Central Europe. *EUMETSAT Meteorological Satellite Conference*, 8–12 September, Darmstadt.

Stensrud DJ, Fritsch JM. 1994a. Mesoscale convective systems in weakly forced large-scale environments. Part II: generation of a mesoscale initial condition. *Mon. Weather Rev.* **122**: 2068–2083.

Stensrud DJ, Fritsch JM. 1994b. Mesoscale convective systems in weakly forced large-scale environments. Part III: numerical simulations and implications for operational forecasting. *Mon. Weather Rev.* **122**: 2084–2104.

Tjemkes S, van de Berg L, Schmetz J. 1997. Warm water vapour pixels over high clouds as observed by METEOSAT. *Beit. Phys. Atmos.* **70**(1): 15–21.

Toth Z, Zhu Y, Marchok T, Tracton MX, Kalnay E. 1998. Verification of the NCEP global ensemble forecasts. *Preprints: 12th Conference on Numerical Weather Prediction*, 11-16 January, Phoenix, AZ. American Meteorological Society: Boston, MA. 286–289.

Vila AD, Machado AL, Laurent H, Velasco I. 2008. Forecast and Tracking the Evolution of cloud clusters (FORTRACC) using satellite infrared imagery: methodology and verification. *Weather Forecast.* **23**: 233–245.

Zipser EJ. 1982. Use of a conceptual model of the life cycle of mesoscale convective systems to improve very-short range forecast. In *Nowcasting*, Browning K (ed.). Academic Press: New York, NY. 191–204.

Zittel WD. 1976. Computer applications and techniques for storm tracking and warning. *Preprints: 17th Conference on Radar Meteorology*, Seattle, WA; 514–521.

